Available online at www.sciencedirect.com
ScienceDirect
C. R. Physique 9 (2008) 389–400
COMPTES RENDUS PHYSIQUE
http://france.elsevier.com/direct/COMREN/

Materials subjected to fast neutron irradiation/Matériaux soumis à irradiation par neutrons rapides

Helium and point defect accumulation: (i) microstructure and mechanical behaviour

Robin Schäublin [a,*], Jean Henry [b], Yong Dai [c]

[a] *École polytechnique fédérale de Lausanne (EPFL), Centre de recherches en physique des plasmas, Association Euratom – Confédération Suisse, CH-5232 Villigen PSI, Switzerland*
[b] *DEN/DMN/SRMA, CEA Saclay, 91191 Gif sur Yvette cedex, France*
[c] *Spallation Neutron Source Division, Paul Scherrer Institut, CH-5252 Villigen PSI, Switzerland*

Available online 11 April 2008

Abstract

Ferritic/martensitic (F/M) steels are good candidate structural materials for the future fusion reactors and spallation sources. However, irradiation of steels is known to produce hardening, loss of ductility, shift in ductile to brittle transition temperature (DBTT) and reduction of fracture toughness and creep resistance starting at low doses. Helium (He), produced by transmutation during the irradiation, also impacts mechanical properties. Numerous experimental and theoretical studies on the evolution of the microstructure of steels under irradiation have been conducted until now. We review the effect of irradiation-induced point defects and in particular of He on the mechanical properties of F/M steels. ***To cite this article: R. Schäublin et al., C. R. Physique 9 (2008).***

Résumé

He et accumulation de défauts ponctuels : (i) microstructure et comportement mécanique. Les aciers ferritiques/martensitiques sont de bons candidats pour les matériaux de structure des futurs réacteurs à fusion et des sources de spallation. Cependant, l'irradiation d'aciers conduit au durcissement, à la perte de ductilité, à la dérive de la température de transition fragile-ductile et à une réduction de ténacité et de résistance au gonflement, et ce, dès les doses les plus faibles. L'hélium (He), produit par transmutation durant l'irradiation, influence ces propriétés. De nombreuses études expérimentales et théoriques sur l'évolution de la microstructure des aciers sous irradiation ont été conduites jusqu'à présent. Nous passons en revue l'effet des dégâts d'irradiation, en particulier de l'He, sur les propriétés mécaniques des aciers ferritiques/martensitiques. ***Pour citer cet article : R. Schäublin et al., C. R. Physique 9 (2008).***

Keywords: Steel; Plasticity; Microstructure; Radiation damage; Helium

Mots-clés : Acier ; Plasticité ; Microstructure ; Dégâts d'irradiation ; Helium

* Corresponding author.
E-mail addresses: robin.schaeublin@psi.ch (R. Schäublin), jean.henry@cea.fr (J. Henry), yong.dai@psi.ch (Y. Dai).

1631-0705/$ – see front matter
doi:10.1016/j.crhy.2008.01.003

1. Introduction

Reduced activation ferritic/martensitic (F/M) steels are good candidate structural materials [1] for future fusion reactors and spallation targets, for, relative to austenitic steels, their excellent thermomechanical properties (high strength, low thermal expansion, high thermal conductivity) and lower damage accumulation and moderate swelling under irradiation. Irradiation of F/M steels, at temperatures below about 400 °C, is known to produce hardening, loss of ductility, shift in ductile to brittle transition temperature (DBTT) and reduction of fracture toughness and creep resistance starting at a dose level of 10^{-2} displacements per atom (dpa), due to the production and accumulation of lattice point defects, which are vacancies and interstitials, and transmutation products, such as hydrogen (H) and helium (He) gases. In future fusion reactors (e.g. in 'DEMO') the plasma facing components will be irradiated with doses corresponding to 20 to 30 dpa per year and will receive heat loads up to 20 MW m^2 [2]. The envisaged upper operating temperature with F/M steels is about 650 °C, with hopes to increase it to 800 °C with the advent of the oxide dispersion strengthened (ODS) F/M steels [3].

The production of He in F/M steels due to 14 MeV fusion neutrons amounts to about 10 to 15 appm per dpa while the H production may reach 40 to 50 appm per dpa, both being much larger than in a fission reactor ($\sim$1 and $\sim$10 appm/dpa, respectively) [4]. While the detrimental effect due to lattice damage, or Wigner disease (in [5]), on the mechanical properties has been recognized a while ago, for example by electron irradiation, the impact of He on those for ferritic material has been a matter of hot debate [6–8], in contrast to austenitic material. Part of the controversy stems from the intimate link between lattice damage and gas production, as any method of introduction of gas in the material will inherently produce self point defects. The effect of H is some times found to be negligible [9], in contrast to [10], but is generally neglected on the grounds that its high diffusivity will lead to its escape out the material through free surfaces [6].

Several methods are used to simulate the He effects expected in spallation neutron sources or fusion reactors. There is the doping by nickel [11], or boron [12], or the replacement of part of Fe by one of its isotopes, ^{54}Fe [13], all yielding larger amounts of He per dpa than with the base material, and the implantation of ions of He, alone or together with H or Fe, using a single-, dual- or triple-beam accelerator [10,14–16]. There is also the use of spallation neutron sources themselves, such as LANSCE [17] and SINQ [18–20], and finally the use of injector foils, as described in [21].

We address in this article some of the cross-cutting issues of paramount importance for the design of safe and tolerant materials of future power plants and accelerator driven systems (ADS) based on very high temperature and high irradiation level cores. We review the effect of irradiation on the microstructure and on the mechanical properties, stressing in particular the effect of He, one of the utmost key issues [11].

2. Materials

Several varieties of F/M steels have been developed around the world for future fusion reactors and spallation sources. To mention only a few, they include the European MANET-I, MANET-II and EUROFER 97, the Japanaese F82H and JLF-1, the Russian RUSFER-EK-181, the American T91, EM10, HT-9 and ORNL 9Cr-2WVTa and the Chinese CLAM. The composition is about 7.5 to 12 wt% Cr, 1 to 2 W, 0.3 to 0.6 Mn, 0.15 to 0.25 V, 0.08 to 0.11 C, minor alloying elements such as Ta, and Fe for the balance. The heat treatments generally include austenization, quench, tempering and air-cooling. The final microstructure consists in tempered martensite. Its matrix is fully ferritic and its morphology, retaining the memory of the martensite, contains a high density of both dislocations and low angle subgrain boundaries, which are the remains of the martensite elongated lath boundaries. During tempering the carbon that was retained in solution in the martensite precipitates in carbides, mainly of the type $Cr_{23}C_6$. These microstructure features contribute to the good mechanical properties of F/M steels.

3. Microstructure

Upon irradiation with either high energy protons or neutrons the ferritic structure of the F/M steels exhibits, in transmission electron microscopy (TEM), starting at low doses, so-called 'black dots', which are 1 to 2 nm in size [22]. This term characterizes diffraction contrasts in the TEM micrograph that are too small to allow for the identification of the crystalline defect at their origin. The difficulty resides in the defect size that is at the limit of the spatial resolution of the TEM used in diffraction contrast, which remains the most suitable technique to image crystal nanometric

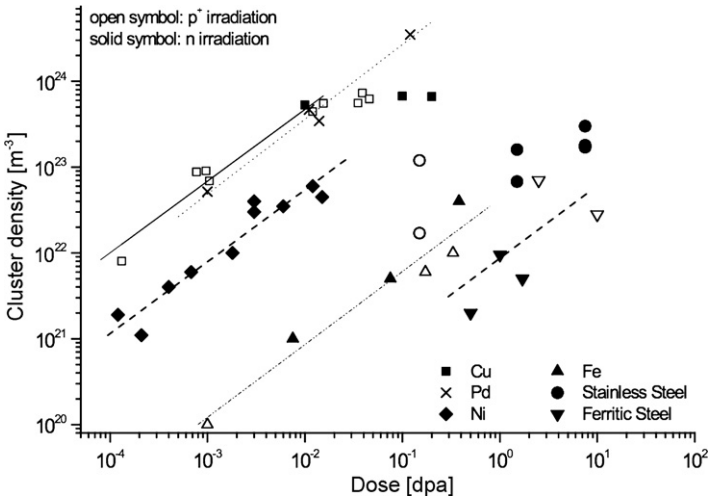

Fig. 1. Defect cluster density as a function of irradiation dose in pure metals and technical alloys [36].

defects. There are new ways to improve on resolution [23], but it will take time to see these applied in this field. With increasing dose the black dots grow to identifiable contrast features. The irradiation-induced defects appear to be dislocation loops, secondary phase precipitates and cavities. Being obstacles to mobile dislocations, the vector of plasticity, they contribute to the degradation of mechanical properties.

It is the dislocation loop that is usually accounted for to estimate changes in mechanical properties. Irradiation induced dislocation loops in ferritic material, which has a body centered crystalline (bcc) structure, have at small sizes a Burgers vector of $1/2a_0\langle 111\rangle$ [24–27] and occasionally $a_0\langle 100\rangle$, as reported in [24]. At larger sizes, beyond about 5 nm, they can present both $1/2a_0\langle 111\rangle$ and $a_0\langle 100\rangle$ Burgers vectors [26,27]. It should be noted that $a_0\langle 100\rangle$ loops are more frequently observed in Fe relative to other bcc metals. They were observed in Mo [28]. Using, for example, the inside-outside contrast technique in TEM, the $a_0\langle 100\rangle$ loops reveals an interstitial nature [26]. At high doses the ferritic/martensitic steel develops a network of dislocations with both $1/2a_0\langle 111\rangle$, which is favoured in the bcc structure [29], and $a_0\langle 100\rangle$ Burgers vectors, the latter being predominant when the Cr content is below that of Fe–6Cr [30]. Irradiation induced dislocations with $a_0\langle 100\rangle$ Burgers vector arise from the growth of $a_0\langle 100\rangle$ interstitial loops [27,30,31]. The Burgers vector of irradiation induced-dislocation loops depends also on irradiation temperature; in Fe at 60 °C it is $1/2a_0\langle 111\rangle$ while at 550 °C it is $a_0\langle 100\rangle$ [32]. With increasing irradiation temperature, but below 300 °C, the dislocation loop structure slightly coarsens; in e.g. F82H at a given dose the loop number density decreases and size increases [33]. From about 300 °C [27] to 350 °C [33–35] this coarsening becomes significant.

Ferritic materials, including F/M steels, exhibit under irradiation, as do other bcc metals, a lower accumulation rate of visible damage than fcc metals and in particular austenitic steels (Fig. 1) [36]. With increasing dose the damage accumulation rate decreases and the microstructure coarsens. There is saturation of the defect density in some cases, by example in Cu in Fig. 1, whilst in ferritic materials such as F/M steels the irradiation-induced microstructure does not seem to have saturated, for the doses examined for Fig. 1. The difference in damage accumulation between bcc and fcc metals is rationalized by the difference in clustering rate of point defects generated during the displacement cascade. At the end of the cascade, in bcc metals the point defects cluster yield is lesser than in fcc [37], as confirmed by MD simulations, in comparing, e.g. Fe versus Cu [38–40]. In addition, one dimensional (1D) migration over three dimensional (3D) migration was identified as a key parameter, as it can explain the defect depleted regions adjacent to grain boundaries ([41], in [42]).

The large variation of results present in the literature should be noted. For instance in the case of Ni, the damage accumulation is found either lower than in other fcc metals [37] or similar [43,44], and some find a significant fraction of SFT relative to loops, while other do not find SFTs [37,45]. It appears clearly that the difference stems from the quality of the observation, owing to their small size. Early microscopes did not have sufficient resolution to reveal nanometric SFTs characteristic contrasts, as in this observation with a Siemens Elmiskop 102 [45].

In F/M steels, irradiation induced precipitation of secondary phase precipitates is often observed [46]. One of the detrimental precipitations expected in steels containing more than about 10% Cr, the composition beyond which the

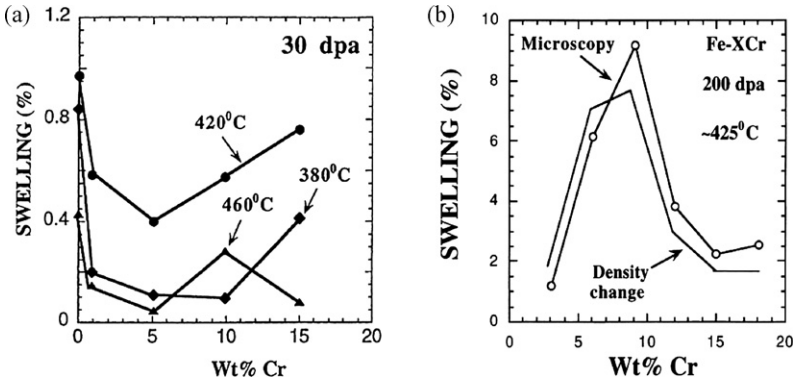

Fig. 2. Swelling of Fe–Cr model alloys as a function of Cr content, showing around 5% Cr (a) a minimum after irradiation in DFR or (b) a maximum after irradiation in FFTF-MOTA (from [51]).

enthalpy of mixing of Fe and Cr becomes positive [47], is the one of pure Cr in the form of α' precipitates. This was recognized and observed in TEM long ago following thermal ageing [48], which leads to the so-called 475 °C embrittlement [49].

Irradiation induced cavities, as voids or gas bubbles, are observed in ferritic material after relatively higher dose than for austenitic steels. This was clearly observed long ago in TEM in a duplex steel [50]. Cavity formation leads to a macroscopic swelling or loss of dimensional stability of the material. Results show a relative good resistance to swelling of the ferritic steels relative to austenitic steels [29,50,51]. While the latter swell at a rate of about 1% for 10 dpa, the former swell at a rate 1% for 100 dpa [29]. However, these values include an incubation dose that ranges from 10 to 100 dpa depending on the irradiation type [51]. In the steady state swelling regime it was noted a swelling rate of 0.2% and 1% per dpa for F/M and austenitic steels, respectively [51]. There is a peak in swelling centered around an irradiation temperature of 400 °C [52] for a damage rate typical of irradiation conditions of cladding tubes in a fast reactor. In addition, a dependency of swelling on composition, such as Cr and Ni contents, is observed. In a binary alloy Fe–Cr and for a Cr content between 0 and 15%, it appears a minimum in swelling centered at 5% Cr following irradiation in reactor [52]. In model Fe–Cr alloys and for DFR reactor irradiations to 30 dpa at temperatures between 380 °C and 460 °C, the same trend is observed, with a minimum in swelling centered at 5% Cr [51]. However, this trend should be taken with caution. It appears that it is inverted (Fig. 2), with a strong maximum in swelling centered around 5 to 10% Cr, when the Fe–Cr alloys are irradiated in FFTF-MOTA reactor [30,51]. The reduction in swelling beyond 10% Cr is attributed to the onset of α' precipitation. The difference appears to be in the irradiation type, or reactor in these cases. Swelling initiates after an incubation time or transient regime [51] that depends on the material, somehow, but certainly on irradiation conditions. After this transient swelling shows a sharp increase [51] before reaching a steady state at low swelling rate that maintains itself up to very high doses [53]. While the situation is rather unclear [53], all hints point towards the role of He, as one of the major differences between irradiation reactors is the He production rate.

We examine in the following the impact of He on swelling. It has been shown that the presence of solute gas atoms, such as O and He [54–56] play an important role in the nucleation of voids as they stabilize the 3-dimensional geometry for a small vacancy cluster which is less stable than the platelet geometry [57]. Ni doped 9Cr–1MoVNb and 12Cr–1MoVW irradiated in HFIR reactor showed higher swelling than in the case of an irradiation in FFTF reactor, attributed to the larger He production per dpa in HFIR [58]. The same conclusion was drawn in a comparison of EBR-II and FFTF irradiation on the swelling of Fe(Cr) model alloys, where EBR-II induces a larger He/dpa ratio [53]. It was also concluded that swelling dependence on dpa rate is weak. F82H doped with boron at different levels was irradiated in HFIR and exhibited a swelling and a number density of cavities proportional to the He content [59].

Following irradiation in SINQ spallation source at temperatures below 360 °C and up to 12 dpa and 1120 appm He, F82H exhibits in TEM nanometric cavities only for doses higher than 5.8 dpa [34], corresponding to temperatures higher than 175 °C and He contents higher than about 750 appm. The cavity size slightly increases with temperature [34]. In T91 steel, nanometric bubbles are observed from 9.1 dpa [60]. In a second SINQ irradiation at temperatures at and below 400 °C (±50 °C) and doses up to 20.3 dpa, F82H shows cavities in two different sizes, reaching 50 nm for the larger ones [33]. The He level reached 1800 appm at 20.3 dpa. The bimodal size distribution is

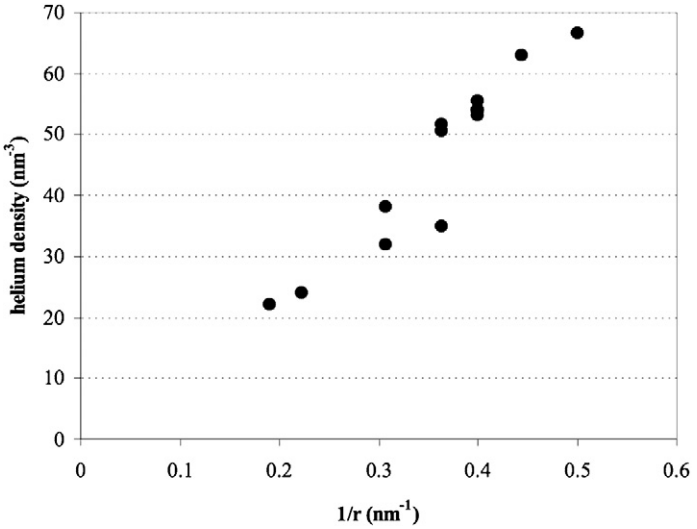

Fig. 3. Helium density as a function of bubble size measured by EELS in a 9Cr–1Mo martensitic steels implanted with 0.5 at% He at 550 °C [73].

attributed to the higher temperature, but He content plays certainly also a role. In all cases, no obvious segregation of cavities on grain boundaries was observed, in contrast to material irradiated in HFIR at 600 °C to about 40 dpa [11]. They locate preferentially at dislocations [33]. It should be noted that in SINQ the H production rate is about a factor of five times higher than that of He. However, the measured H content in samples irradiated at temperatures above 250 °C is 300 to 400 appm, which is not much higher than that of unirradiated samples, at about 200 appm. For samples irradiated below about 150 °C the measured H concentrations is quite close to calculated ones. This indicates that H diffused out of the samples during irradiation at high temperatures [19], as can be expected because H is a fast diffuser in ferritic materials, relative to austenitic steel [61]. Therefore, it is believed that H, relative to He, should not contribute much to cavities observed in the samples irradiated at higher temperatures to higher doses. It should be noted that while only 10% of the generated H was detected in some SINQ irradiated specimens [19], it represents a significant amount of gas, comparable to the He content within a factor of 2, whose still unclear impact could be significant [62].

There have been a number of studies regarding helium effects on the microstructural evolution of Cr martensitic steels using He implantation experiments or so-called 'dual-beam' experiments, whereby He is injected while the specimen is being simultaneously irradiated with Fe ions in order to create displacement damage. It allows adjusting the appm He/dpa ratio to a chosen value, as in [63–66]. For example, ion implantation of He to 5000 appm into EM10 and 9Cr–1Mo to 250 and 550 °C [16] produces cavities that are visible only at 550 °C using TEM [67]. Note that the implantation corresponds to an irradiation dose and dose rate of 0.8 dpa and 2.5×10^{-6} dpa s^{-1}, respectively [16]. In this case there is clear evidence of cavities at grain boundaries [67]. Increasing the He injection rate at a given temperature and total He content, or decreasing the implantation temperature with implantation rate and accumulated He quantity kept constant, result in the decrease of the average He bubble sizes and increase in the bubble number densities. At higher He implantation temperatures, typically above $0.4T_m$, where T_m is the melting temperature, bubble nucleation in martensitic steels occurs preferentially on dislocation, martensitic lath and grain boundaries and precipitates. Bubbles tend to be elongated and strongly faceted [66–68], with facets parallel to {100} planes. At lower temperatures and/or high implantation rates the tiny nanometric bubbles that are created appear spherical when characterized by means of conventional TEM techniques. However a recent study revealed, using holography in a TEM, that these small bubbles may be actually facetted as well [69]. Some attempts have also been made to evaluate the He density inside bubbles using techniques such as small angle neutron scattering (SANS) [67,70] and electron energy loss spectroscopy (EELS) [71]. However, they simultaneously sample a number of bubbles that may come in various sizes, He contents and pressures. More recently, an experimental procedure based on EELS measurements was devised that allows determining the He density of a single bubble [72]. This procedure was used to characterize bubbles in an He-implanted 9Cr–1Mo martensitic steel (Fig. 3) [73]. The pressure inside the bubbles was found to be somewhat lower that the equilibrium pressure derived from Trinkaus' equation of state for He [74]. This tech-

nique should prove very useful in the future in order to determine He densities in bubbles and voids as a function of implantation/irradiation conditions.

Furthermore, following dual-beam irradiation, a bimodal cavity size distribution may occur in a given temperature range which depends on the irradiation conditions (see for instance [63,64]). The larger cavities contain a He density below equilibrium pressure. Such voids appear when a helium bubble reaches a critical size/gas content beyond which the cavity begins to grow more quickly as a result of an excess flux of vacancies over interstitials, due to a bias in the point defect elimination at sinks [75]. However, it should be noted that the effect of the irradiation parameters on void swelling and in particular the role of the He/dpa ratio and of the helium generation rate have not been studied in detail so far in F/M steels. The effect may likely be non-linear as in the case of austenitic steels. It was shown that for a given dpa level and damage rate, swelling increases with increasing He/dpa ratio and then decreases beyond a critical value of this ratio [76]. More effort is needed, using a combination of experiments and modelling activities, in order to assess whether for spallation- and fusion-relevant irradiation conditions, void swelling in F/M steels would reach values of concern regarding dimensional stability and mechanical properties.

4. Mechanical properties

We start with a description of the general effects of irradiation on the mechanical properties of F/M steels, before entering into the details of the effect of He on these. While at 450 °C and beyond, the mechanical properties of FM steels seem relatively unaffected by irradiation, below this temperature the irradiation-induced lattice damage induces strong hardening [77]. It is accompanied by a strong loss of ductility and a shift in DBTT. In a range of F/M steels irradiated at 300 °C the hardening and loss of ductility rates start to decline from about 3 to 5 dpa and there is saturation at 10 dpa [78] while the DBTT shift rate does not seem to clearly decline up about 10 dpa [78,79]. It should be noted that the shift in DBTT shows a strong dependency with the Cr content (Fig.4) [7], with a minimum at about 8 to 10% Cr for FM steels irradiated below 450 °C.

The high helium generation rates in fusion and spallation environments are a prime concern due to their potential deleterious effects on mechanical properties. It was recognized several years ago that He might significantly degrade the high temperature creep strength of metals. This is the so-called 'high temperature helium embrittlement' phenomenon, which typically occurs at $T > 0.4T_m$ [80]. This phenomenon was studied by performing high temperature creep tests on miniature specimens either pre-implanted with He or tested during helium implantation [66,68]. Reductions of time/strain to fracture up to several orders of magnitude were observed together with a change of fracture mode from transgranular to intergranular. The degradation of the creep properties results from the nucleation of He bubbles

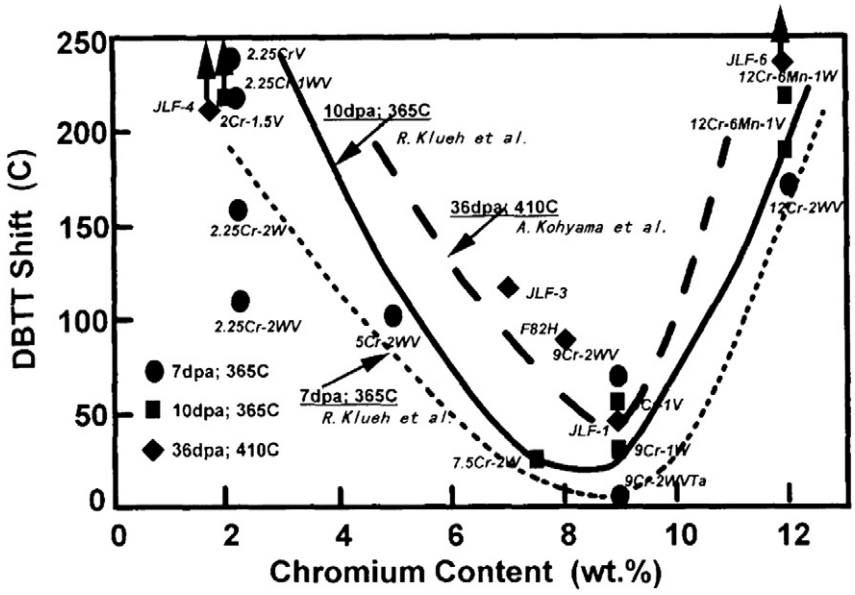

Fig. 4. Effect of chromium content on the DBTT shift of F/M steels irradiated in FFIF (from [7]).

on grain boundaries, their growth by He absorption and transformation to voids above a critical radius, followed by coalescence inducing crack formation and fracture [81]. Furthermore, the F/M steels have been shown to be much more resistant to high temperature embrittlement than austenitic steels, as explained in detail in [68].

By contrast, helium effect on hardening and embrittlement at temperatures below $0.4T_m$ was, until to recently, less clear and somewhat controversial [82]. The tensile stress–strain curves of FM steels after irradiation in fission reactors (e.g. [17]) and in spallation targets [62,83–85] are rather similar. In cases of low irradiation doses, below about 10 dpa, and low He concentrations, below about 1000 appm, the He effect on hardening is not obvious [17]. After irradiation, the uniform elongation may drop below 1%, demonstrating substantial embrittlement. For FM steels, the most concerned issue is the shift of DBTT (ΔDBTT) after irradiation in low temperature regime. For neutron irradiated FM steels, the ΔDBTT is generally proportional to the hardening ($\Delta\sigma y$) and saturates at about 10 dpa while for FM steels irradiated in SINQ targets, the ΔDBTT does not [16] saturate at doses up to 20 dpa [86,87]. The additional increase of DBTT at doses larger than 10 dpa is believed to be due to He embrittlement effect, which is referred to as non-hardening embrittlement effect of He [82].

Moreover, recent results have indicated that helium may have at low temperature a dramatic impact on the mechanical properties of FM steels. For instance, 0.5 at% He implanted at 250 °C in miniature tensile specimens of 9Cr–1Mo martensitic steels induced high hardening, complete loss of ductility together with a fully intergranular fracture mode [16,88]. It is believed that this fracture mode results from the combined effects of drastic hardening due to a high density of implantation-induced He bubbles and point defect clusters and weakening of grain boundaries by He [67]. Electronic structure calculations confirm that the presence of He at a grain boundary significantly reduces its cohesion [89,90]. The same 9Cr–1Mo martensitic steels were irradiated in the SINQ spallation target at a maximum irradiation temperature of 360 °C up to 20 dpa which corresponds to a He content close to 0.2 at% [91]. The specimens irradiated to the highest doses/He concentrations broke in a brittle manner and displayed a predominantly intergranular fracture mode, while the specimens irradiated to lower doses, although significantly embrittled by the irradiation, retained a ductile behaviour. Miniature Charpy specimens were implanted in the notch region to 0.125 and 0.25 at% He at 250 and 400 °C and subsequently submitted to static bending tests [92–94]. Brittle fracture initiation and propagation in the implanted zones were systematically recorded and the fracture surfaces displayed significant amounts of intergranular separation. Based on finite element analysis of the tests, it was shown that He induced a decrease in the critical stress for intergranular fracture. The fracture toughness was evaluated using the Beremin model for brittle fracture [94]. The toughness at room temperature after implantation dropped to 16 MPa $m^{1/2}$, i.e. below the value measured at low temperature (−170 °C) in the brittle domain for the as-received steel.

5. Modeling

Modeling constitutes nowadays a major tool in the investigation of radiation damage effects. Multiscale modeling, besides experiments, appears in this context a major player as it allows one to establish solid foundations to the understanding of the relationship between irradiation damage and the induced mechanical response of the target material, starting at the atomic scale. Molecular dynamics simulations is one of the techniques that is largely used in this field as it allows an atomistic description of the generation of the damage by irradiation and of the interaction of dislocations with irradiation-induced defects. MD is limited by the availability and accuracy of empirical interatomic potentials capable to describe the alloying elements present in the F/M steels. At present, many simulations are conducted in pure Fe. Here we focus mainly on MD simulation results.

We present results on the primary state of damage in Fe and Fe alloys. MD simulations using empirical potentials and ab initio calculations [95,96] recently coincide in indicating that in α-Fe, unlike other bcc transition metals [96], the $\langle 110\rangle$ dumbbell as the most stable SIA, followed by $\langle 111\rangle$ dumbbell, which in turn is very close to the $\langle 111\rangle$ crowdion. It should be noted that experiments using Huan scattering with X-rays and early simulations indicated that in all bcc metals, such as Mo and Fe, $\langle 110\rangle$ dumbbells are the most stable self-interstitials. The configuration of the $\langle 110\rangle$ dumbbell in bcc can be obtained through a simple geometrical transformation of the $\langle 100\rangle$ dumbbell in fcc, where it is the most stable self interstitial, by a slight compression along one $\langle 100\rangle$ axis, akin to the diffusionless martensitic transformation. Assuming the physics is similar, the geometrical similarity supports the $\langle 110\rangle$ dumbbell in bcc structure as the most stable SIA.

It was postulated long ago that the $\langle 110\rangle$ dumbbells aggregate to form $1/2a_0\langle 110\rangle$ loops [97]. Ab initio calculations [95] indicate that in Fe the $\langle 110\rangle$ interstitial clusters should form $1/2a_0\langle 110\rangle$ loops when they are smaller than 4 to 5

self interstitials, while at larger sizes the Burgers vector $1/2a_0\langle 111\rangle$ should dominate. It can be explained by the high stacking fault energy in the $1/2a_0\langle 110\rangle$ loops, which makes them unfavourable. They can transform to $1/2a_0\langle 111\rangle$ loops or even to the least energetically favourable $a_0\langle 100\rangle$ loops through the Eyre–Bullough shearing mechanism [97]. Another mechanism of transformation was recently derived by MD simulation in Fe [98]. It should be noted that a small amount of tensile strain, from 0.1%, applied during the MD simulation of a cascade changes the resulting SIA population to one with a majority of $\langle 111\rangle$ dumbbells [99]. The stability of $\langle 110\rangle$ dumbbell as single SIA or in cluster should be further studied by simulation. It should be noted that, in vanadium, another bcc metal, experiments have shown small $1/2a_0\langle 110\rangle$ loops [100], despite the large stacking fault energy, while ab initio simulations indicate $\langle 111\rangle$ as the most stable interstitial [96].

MD simulations show that the defect yield, N_f, induced by cascades is smaller than that predicted by the NRT model [101] with $N_f = 0.8E_p/(2E_d)$, where E_p is the incident energy and E_d is the displacement threshold energy, and follows rather $N_f = A(E_p)^m$ [102], where A and m are weakly dependent on the material, as in Fe [103] and Ni [104]. It seems, however, to depend on atomic weight and melting point. Point defects clustering induced directly by cascades is commonly observed in MD simulations, e.g. in Cu [105]. The type of clustering, i.e. the clusters' nature, size, morphology and spatial distribution, is critical for the long term evolution of the microstructure, as simulated by kinetic Monte Carlo in Fe [106]. However, results on clustering show large variations depending on the potential, in Fe [103,107] as well as in fcc metals such as Cu [105] and Ni [108].

We present results on radiation-induced precipitation. Fe–Cr potentials are needed in order to model radiation damage in a system closer to F/M steels, if one intends to study α' precipitation for instance. Recently, two different interatomic potentials for Fe–Cr were developed [109,110], which reproduce the change in sign of the heat of mixing of the Fe–Cr system at 10% Cr [47]. One of these potentials [110] was used to simulate the damage production in Fe(Cr) [111], showing that the content in Cr does not cause drastic changes in the cascade efficiency relative to a pure Fe. No clustering of Cr is observed. A fraction of Cr atoms remains in interstitial position after the cool down of the cascade, an effect that could influence the long-term evolution of the microstructure. Similarly in Fe(Cu) there is no drastic effect of the displacement cascade, e.g. on the Cu spatial distribution, but the few binding between isolated Cu atoms and di-vacancies, which could also influence the long-term evolution of the microstructure [38]. In fcc Al(Ni) where Ni rich precipitates are formed under irradiation [112], conversely, MD simulations show that Ni atoms do change the cascade efficiency by increasing it [113], presumably because of the large difference in atomic mass with Al. Pre-existent Ni-rich nanometric precipitates are dissolved by the cascade [113], by ballistic mixing. The Ni atoms are moved towards interstitial sites in the Al lattice [104].

Molecular dynamics simulations of the primary state of damage in Fe(He) show that the presence of He in interstitial sites promote the formation of self interstitial atom clusters [114]. Their number and size is drastically increased when compared to the case of pure Fe or Fe with He in substitutional sites [114,115]. In the latter case, the number and size of vacancy clusters increase while the ones of SIAs decrease relative to pure Fe [115]. In the case when He is interstitial, it tends to combine with SIAs [114]. This feature may drastically reduce the mobility of interstitial clusters relative to pure Fe, with significant impact on the subsequent evolution of radiation-induced defects in the alloy. In effect, vacancy clusters would grow more easily due to the reduced annihilation rate. This in turn will have a significant impact on mechanical properties.

MD simulations allow investigating plasticity in e.g. the simulation of the interaction of the passage of one dislocation through a defect [116]. Note that, akin to cascade simulations, these simulations are dependent on the chosen interatomic potential [116,117]. A major issue in simulating by MD the dislocation glide in bcc structure is the mobility of the screw dislocation with its three-fold symmetry core [116,118]. Voids appear to be the strongest obstacles to moving dislocations [119–121]. He in solid solution does not have a significant effect on the yield stress before it reaches 1.0 at% He [119]. A 2 nm void presents an obstacle strength of 590 MPa to the passage of an edge dislocation [119]. In contrast, a 2 nm He bubble is a weaker obstacle than the void when the He content is low, at 1 to 2 He atoms per vacancy [119]. Beyond 2 He atoms per vacancy, a content at which the bubble is the weakest, the resistance of the He bubble increases with increasing He content. At 5 He atoms per vacancy, the He bubble becomes a much stronger obstacle, which is due to significant loop punching [119], which stochastic nature induces scatter in the resulting obstacle strength [122]. With increasing temperature the cavity obstacle strength decreases [123]. In the literature there is experimental evidence of gas bubble induced loop punching, such as for H bubbles in Cu [124] and He bubbles in Al–0.4Li [125]. Ab initio calculations suggest that such an effect might be also effective in Fe, as they show that up to 4 He atoms strongly bind with a single vacancy [126], which would lead to pressurized He

bubbles that could release their pressure by emitting self interstitial atoms. This so-called self-trapping of He [127] was however to our knowledge never observed experimentally in ferritic materials.

6. Summary

Following irradiation pure α-Fe and ferritic/martensitic steels present in the microstructure undefined small clusters appearing as black dots in TEM, dislocation loops with Burgers' vector of mainly $1/2a_0\langle 111\rangle$ and $a_0\langle 100\rangle$, the latter rarely appearing in other bcc metals, and cavities. Secondary phase precipitation is also observed, in particular the one of pure Cr or α'. Spallation reaction due to intranuclear cascades gives rise to impurities, mainly H and He gases. While the role of H remains unclear, there is a clear impact of He on the microstructure, promoting the growth of cavities, which can be more or less pressurized by He.

There is a strong hardening, loss of ductility and increase in DBTT following irradiation. This trend is dependent on irradiation conditions, material and He content. A drastic reduction in them appears for Tirr $\geqslant$450 °C. Their increase with increasing dose starts to decline from 3 to 5 dpa and there is a trend to saturation from 10 dpa. It appears that there is a strong dependency of DBTT on Cr content, with a minimum in ΔDBTT between 8 to 10% wt Cr. He seems to induce embrittlement, in some cases without measurable hardening, and the saturation trend in the ΔDBTT is not observed when He is present.

Modeling by ab initio and molecular dynamics simulations proves very fruitful in expanding our understanding on radiation damage and in particular on the role played by He. Mechanical properties do benefit also from simulations, in particular MD simulation. Recent ab initio simulations indicate that the SIA in α-Fe is $\langle 110\rangle$, while other bcc transition metals should have a $\langle 111\rangle$ SIA. This is in contrast with early experimental results that indicated that the SIA in bcc metals is $\langle 110\rangle$. Of course, one should consider the limits of the experimental methods and the precision of the ab initio calculations in making such a comparison. This point, however, which is critical for understanding the long-term evolution of the microstructure, should be further investigated. MD simulations indicate that the location of the He atoms in the lattice is critical to understand the synergies between point defects leading to the evolution of the microstructure under irradiation. In the case He atoms are on interstitial sites the simulated cascades result, relative to pure Fe, in an increase in the number of self interstitials while for substitutional He atoms there is an increase in the vacancy number.

MD simulations in α-Fe of the passage of an edge dislocation through a defect indicate that the void is the strongest obstacle, relative to a Cu precipitate, a $a_0\langle 100\rangle$ loop and a He bubble with low He content. Indeed, it appears that for low He contents the cavity is surprisingly weak, weaker than the void, while for high He content the cavity starts to emit dislocation loops, thus forming a strong obstacle to the dislocation. The strength of the cavity as obstacle relies then entirely on its He content.

Acknowledgements

D. Gelles is thanked for fruitful discussions. EFDA is acknowledged for financial support and the Paul Scherrer Institute is acknowledged for the overall use of the facilities.

References

[1] N. Baluc, R. Schaublin, P. Spatig, M. Victoria, Nuclear Fusion 44 (2004) 56–61.
[2] A. Moslang, E. Diegele, M. Klimiankou, R. Lasser, R. Lindau, E. Lucon, E. Materna-Morris, C. Petersen, R. Pippan, J.W. Rensman, M. Rieth, B. van der Schaaf, H.C. Schneider, F. Tavassoli, Nuclear Fusion 45 (2005) 649–655.
[3] S.J. Zinkle, N.M. Ghoniem, Fusion Engineering and Design 51 (2) (2000) 55–71.
[4] M.S. Wechsler, D.R. Davidson, L.R. Greenwood, W.F. Sommer, Effects of Radiation on Materials: 12th conference, ASTM, 1985.
[5] Y. Quéré, in : La sagesse du physicien, L'oeil neuf, Paris, 2005, p. 34.
[6] H. Schroeder, H. Ullmaier, Journal of Nuclear Materials 179–181 (1991) 118–124.
[7] A. Kohyama, A. Hishinuma, D.S. Gelles, R.L. Klueh, W. Dietz, K. Ehrlich, Journal of Nuclear Materials 237 (1996) 138–147.
[8] D.S. Gelles, Journal of Nuclear Materials 283 (2000) 838–840.
[9] K.K. Bae, K. Ehrlich, A. Moslang, Journal of Nuclear Materials 191 (1992) 905–909.
[10] E.H. Lee, J.D. Hunn, G.R. Rao, R.L. Klueh, L.K. Mansur, Journal of Nuclear Materials 272 (1999) 385–390.
[11] R.L. Klueh, N. Hashimoto, M.A. Sokolov, P.J. Maziasz, K. Shiba, S. Jitsukawa, Journal of Nuclear Materials 357 (2006) 169–182.
[12] K. Shiba, A. Hishinuma, Journal of Nuclear Materials 283 (2000) 474–477.

[13] E. Lucon, P. Benoit, P. Jacquet, E. Diegele, R. Lasser, A. Alamo, R. Coppola, F. Gillemot, P. Jung, A. Lind, S. Messoloras, P. Novosad, R. Lindau, D. Preininger, M. Klimiankou, C. Petersen, M. Rieth, E. Materna-Morris, H.C. Schneider, J.W. Rensman, B. van der Schaaf, B.K. Singh, P. Spaetig, Fusion Engineering and Design 81 (2006) 917–923.
[14] L.K. Mansur, E.H. Lee, P.J. Maziasz, A.P. Rowcliffe, Journal of Nuclear Materials 143 (1986) 633–646.
[15] Y. Katoh, M. Ando, A. Kohyama, Journal of Nuclear Materials 323 (2003) 251–262.
[16] P. Jung, J. Henry, J. Chen, J.C. Brachet, Journal of Nuclear Materials 318 (2003) 241–248.
[17] K. Farrell, T.S. Byun, Journal of Nuclear Materials 318 (2003) 274–282.
[18] G.S. Bauer, Y. Dai, W. Wagner, Journal De Physique IV 12 (2002) 3–26.
[19] Y. Dai, Y. Foucher, M.R. James, B.M. Oliver, Journal of Nuclear Materials 318 (2003) 167–175.
[20] W. Wagner, Y. Dai, H. Glasbrenner, M. Grosse, E. Lehmann, Nuclear Instruments & Methods in Physics Research Section A – Accelerators Spectrometers Detectors and Associated Equipment 562 (2006) 541–547.
[21] G.R. Odette, Journal of Nuclear Materials 143 (1986) 1011–1017.
[22] R. Schaublin, M. Victoria, Journal of Nuclear Materials 283 (2000) 339–343.
[23] R. Schaublin, Microscopy Research and Technique 69 (2006) 305–316.
[24] M.L. Jenkins, C.A. English, B.L. Eyre, Philosophical Magazine A 38 (1978) 97–114.
[25] A.C. Nicol, M.L. Jenkins, M.A. Kirk, Matrix damage in iron, in: Materials Research Society Symposium – Proceedings, 2001.
[26] R. Schaeublin, M. Victoria, Identification of defects in ferritic/martensitic steels induced by low dose irradiation, in: Microstructural Processes in Irradiated Materials, Materials Research Society, Boston, 2001.
[27] R. Schaeublin, D. Gelles, M. Victoria, Journal of Nuclear Materials 307 (2002) 197–202.
[28] C.A. English, B.L. Eyre, S.M. Holmes, Journal of Physics F – Metal Physics 10 (1980) 1065–1080.
[29] E.A. Little, Journal of Nuclear Materials 87 (1979) 11–24.
[30] D.S. Gelles, Journal of Nuclear Materials 108 (1982) 515–526.
[31] D.S. Gelles, R.E. Schaublin, Materials Science and Engineering A – Structural Materials Properties Microstructure and Processing 309 (2001) 82–86.
[32] R. Bullough, R.C. Perrin, Proceedings of the Royal Society A 305 (1967) 541–552.
[33] X. Jia, Y. Dai, Journal of Nuclear Materials 356 (2006) 105–111.
[34] X. Jia, Y. Dai, M. Victoria, Journal of Nuclear Materials 305 (2002) 1–7.
[35] X. Jia, Y. Dai, Journal of Nuclear Materials 318 (2003) 207–214.
[36] N. Baluc, C. Bailat, Y. Dai, M.I. Luppo, R. Schaublin, M. Victoria, A comparison of the microstructure and tensile behaviour of irradiated fcc and bcc metals, in: Microstructural Processes in Irradiated Materials, Materials Research Society, 1999.
[37] B.N. Singh, J.H. Evans, Journal of Nuclear Materials 226 (1995) 277–285.
[38] D.J. Bacon, A.F. Calder, F. Gao, V.G. Kapinos, S.J. Wooding, Nuclear Instruments & Methods in Physics Research Section B – Beam Interactions with Materials and Atoms 102 (1995) 37–46.
[39] T.D. de la Rubia, M.J. Caturla, E.A. Alonso, N. Soneda, M.D. Johnson, Radiation Effects and Defects in Solids 148 (1999) 95–126.
[40] M.J. Caturla, N. Soneda, E. Alonso, B.D. Wirth, T.D. de la Rubia, J.M. Perlado, Journal of Nuclear Materials 276 (2000) 13–21.
[41] B.N. Singh, S.J. Zinkle, Journal of Nuclear Materials 217 (1994) 161–171.
[42] M. Kiritani, N.M. Ghoniem, S. Ishino, T.D. de la Rubia, M. Kiritani, B.N. Singh, E. Kuramoto, H.L. Heinisch, S.J. Zinkle, C.H. Woo, P. Vajda, S.I. Golubov, R.E. Stoller, H. Wollenberger, Y. Kato, N. Yoshida, H. Matsui, M. Victoria, J.N. Yu, Journal of Nuclear Materials 272 (1999) 540–552.
[43] Z. Yao, R. Schaublin, M. Victoria, Journal of Nuclear Materials 323 (2003) 388–393.
[44] M. Kiritani, Journal of Nuclear Materials 216 (1994) 220–264.
[45] R. Schindler, W. Frank, M. Ruhle, A. Seeger, M. Wilkens, Journal of Nuclear Materials 69 (7) (1978) 331–340.
[46] R.L. Klueh, D.R. Harries, in: High-Chromium Ferritic and Martensitic Steels for Nuclear Applications, ASTM, West Conshohocken, PA, 2001.
[47] P. Olsson, I.A. Abrikosov, L. Vitos, J. Wallenius, Journal of Nuclear Materials 321 (2003) 84–90.
[48] R.M. Fisher, E.J. Dulis, K.G. Carroll, Transactions of the American Institute of Mining and Metallurgical Engineers 197 (1953) 690–695.
[49] R.O. Williams, H.W. Paxton, Transactions of the American Institute of Mining and Metallurgical Engineers 212 (1958) 422–423.
[50] W.G. Johnston, Jh. Rosolows, A.M. Turkalo, T. Lauritze, Journal of Nuclear Materials 54 (1974) 24–40.
[51] F.A. Garner, M.B. Toloczko, B.H. Sencer, Journal of Nuclear Materials 276 (2000) 123–142.
[52] E.A. Little, D.A. Stow, Journal of Nuclear Materials 87 (1979) 25–39.
[53] F.A. Garner, D.S. Gelles, L.R. Greenwood, T. Okita, N. Sekimura, W.G. Wolfer, Journal of Nuclear Materials 329 (33) (2004) 1008–1012.
[54] L.D. Glowinski, J.M. Lanore, C. Fiche, Y. Adda, Journal of Nuclear Materials 61 (1976) 41–52.
[55] S.J. Zinkle, E.H. Lee, Metallurgical Transactions A – Physical Metallurgy and Materials Science 21 (1990) 1037–1051.
[56] S.J. Zinkle, W.G. Wolfer, G.L. Kulcinski, L.E. Seitzman, Philosophical Magazine A – Physics of Condensed Matter Structure Defects and Mechanical Properties 55 (1987) 127–140.
[57] S.J. Zinkle, L.E. Seitzman, W.G. Wolfer, Philosophical Magazine A – Physics of Condensed Matter Structure Defects and Mechanical Properties 55 (1987) 111–125.
[58] P.J. Maziasz, R.L. Klueh, J.M. Vitek, Journal of Nuclear Materials 141–143 (1986) 929–937.
[59] E. Wakai, N. Hashimoto, Y. Miwa, J.P. Robertson, R.L. Klueh, K. Shiba, S. Jistukawa, Journal of Nuclear Materials 283–287 (2000) 799–805.
[60] X. Jia, Y. Dai, Journal of Nuclear Materials 343 (2005) 212–218.
[61] T.P. Peng, C.J. Alstetter, Acta Materialia 34 (1986) 1771.
[62] J. Henry, X. Averty, Y. Dai, P. Lamagnere, J.P. Pizzanelli, J.J. Espinas, P. Wident, Journal of Nuclear Materials 318 (2003) 215–227.

[63] K. Farrell, E. Lee, Ion bombardment damage in a modified Fe–9Cr–1Mo steel, in: Effects of Radiations on Materials: 12th International Conference, ASTM, 1985.
[64] D. Gilbon, C. Rivera, Journal of Nuclear Materials 155 (1988) 1268–1273.
[65] N. Wanderka, E. Camus, H. Wollenberger, Microstructure evolution of selected ferritic-martensitic steels under dual-beam irradiation, in: Microstructure Evolution During Irradiation, MRS, 1996.
[66] A. Moslang, D. Preininger, Journal of Nuclear Materials 155 (1988) 1064–1068.
[67] J. Henry, M.H. Mathon, P. Jung, Journal of Nuclear Materials 318 (2003) 249–259.
[68] H. Schroeder, H. Ullmaier, Journal of Nuclear Materials 179 (1991) 118–124.
[69] E. Snoeck, J. Majimel, M.O. Ruault, M.J. Hytch, Journal of Applied Physics 100 (2006).
[70] Q. Li, W. Kesternich, H. Schroeder, D. Schwahn, H. Ullmaier, Acta Metallurgica Et Materialia 38 (1990) 2383–2392.
[71] W. Jäger, R. Manzke, H. Trinkaus, R. Zeller, J. Fink, G. Crecelius, Radiation Effects and Defects in Solids 78 (1983) 315–325.
[72] C.A. Walsh, J. Yuan, L.M. Brown, Philosophical Magazine A – Physics of Condensed Matter Structure Defects and Mechanical Properties 80 (2000) 1507–1543.
[73] S. Fréchard, M. Kociak, M. Walls, J.-P. Chevalier, J. Henry, Journal of Nuclear Materials (2007).
[74] H. Trinkaus, Radiation Effects and Defects in Solids 78 (1983) 189–211.
[75] L.K. Mansur, E.H. Lee, Journal of Nuclear Materials 179–181 (1991) 162.
[76] Y. Katoh, R.E. Stoller, Y. Kohno, A. Kohyama, Journal of Nuclear Materials 210 (1994) 290–302.
[77] R.L. Klueh, J.M. Vitek, Journal of Nuclear Materials 182 (1991) 230–239.
[78] E. Lucon, R. Chaouadi, M. Decreton, Journal of Nuclear Materials 329 (33) (2004) 1078–1082.
[79] J. Rensman, E. Lucon, J. Boskeljon, J. van Hoepen, R. den Boef, P. ten Pierick, Journal of Nuclear Materials 329 (33) (2004) 1113–1116.
[80] H. Ullmaier, H. Trinkaus, Materials Science Forum 97–99 (1992) 451–472.
[81] H. Trinkaus, B.N. Singh, Journal of Nuclear Materials 323 (2003) 229–242.
[82] T. Yamamoto, G.R. Odette, H. Kishimoto, J.W. Rensman, Journal of Nuclear Materials 356 (2006) 27–49.
[83] Y. Dai, S.A. Maloy, G.S. Bauer, W.F. Sommer, Journal of Nuclear Materials 283–287 (2000) 513–517.
[84] S.A. Maloy, M.R. James, G. Willcutt, W.F. Sommer, M.A. Sokolov, L.L. Snead, M.L. Hamilton, F.A. Garner, Journal of Nuclear Materials 296 (2001) 119–128.
[85] Y. Dai, X.J. Jia, K. Farrell, Journal of Nuclear Materials 318 (2003) 192–199.
[86] Y. Dai, P. Marmy, Journal of Nuclear Materials 343 (2005) 247–252.
[87] Y. Dai, Journal of Nuclear Materials (2007).
[88] J. Henry, P. Jung, J. Chen, J.C. Brachet, Journal De Physique IV 12 (2002) 103–120.
[89] R. Smith, W. Geng, C. Geller, R. Wu, A. Freeman, Scripta Materialia 43 (2000) 957–961.
[90] C.C. Fu, Annual report of the association EURATOM-CEA, 2006.
[91] J. Henry, X. Averty, Y. Dai, J.P. Pizzanelli, Journal of Nuclear Materials, doi:10.1016/jnucmat.2008.02.027.
[92] J. Henry, L. Vincent, X. Averty, B. Marini, P. Jung, Journal of Nuclear Materials 356 (2006) 78–87.
[93] J. Henry, L. Vincent, X. Averty, B. Marini, P. Jung, Journal of Nuclear Materials 367 (2007) 411–416.
[94] J. Malaparte, L. Vincent, X. Averty, J. Henry, B. Marini, Engineering and Fracture Mechanics, doi:10.1016/j.engfracmech.2007.02.019.
[95] F. Willaime, C.C. Fu, M.C. Marinica, J. Dalla Torre, Nuclear Instruments & Methods in Physics Research Section B – Beam Interactions with Materials and Atoms 228 (2005) 92–99.
[96] D. Nguyen-Manh, A.P. Horsfield, S.L. Dudarev, Physical Review B 73 (2006).
[97] B.L. Eyre, R. Bullough, Philosophical Magazine 12 (1965) 31.
[98] J. Marian, B.D. Wirth, J.M. Perlado, Physical Review Letters 88 (2002).
[99] F. Gao, D.J. Bacon, P.E.J. Flewitt, T.A. Lewis, Nuclear Instruments and Methods in Physics Research Section B: Beam Interactions with Materials and Atoms 180 (2001) 187–193.
[100] P.M. Rice, S.J. Zinkle, Journal of Nuclear Materials 258–263 (1998) 1414–1419.
[101] M.J. Norgett, M.T. Robinson, I.M. Torrens, Nuclear Engineering and Design 33 (1975) 50–54.
[102] D.J. Bacon, A.F. Calder, F. Gao, V.G. Kapinos, S.J. Wooding, Nuclear Instruments and Methods in Physics Research Section B: Beam Interactions with Materials and Atoms 102 (1995) 37–46.
[103] L. Malerba, Journal of Nuclear Materials 351 (2006) 28–38.
[104] A. Cuenat, R. Gotthardtt, R. Schaeublin, Philosophical Magazine 85 (2005) 737–743.
[105] Y.N. Osetsky, D.J. Bacon, Nuclear Instruments and Methods in Physics Research Section B: Beam Interactions with Materials and Atoms 180 (2001) 85–90.
[106] C.S. Becquart, A. Souidi, C. Domain, M. Hou, L. Malerba, R.E. Stoller, Journal of Nuclear Materials 351 (2006) 39–46.
[107] D. Terentyev, C. Lagerstedt, P. Olsson, K. Nordlund, J. Wallenius, C.S. Becquart, L. Malerba, Journal of Nuclear Materials 351 (2006) 65–77.
[108] Z. Yao, M.J. Caturla, R. Schaublin, Journal of Nuclear Materials 367–370 (1) (2007) 298–304.
[109] A. Caro, D.A. Crowson, M. Caro, Physical Review Letters 95 (2005) 075702.
[110] P. Olsson, J. Wallenius, C. Domain, K. Nordlund, L. Malerba, Physical Review B 72 (2005) 214119.
[111] D.A. Terentyev, L. Malerba, R. Chakarova, K. Nordlund, P. Olsson, M. Rieth, J. Wallenius, Journal of Nuclear Materials 349 (2006) 119–132.
[112] R. Schaublin, R. Gotthardt, Radiation Effects and Defects in Solids 126 (1993) 185–188.
[113] A. Cuenat, R. Schaublin, A. Hessler-Wyser, R. Gotthardt, Ultramicroscopy 83 (2000) 179–191.
[114] J. Yu, Z. Yao, G. Yu, R. Schaeublin, Journal of Nuclear Materials 367–370 (1) (2007) 462–467.
[115] L. Yang, X.T. Zu, H.Y. Xiao, F. Gao, H.L. Heinisch, R.J. Kurtz, K.Z. Liu, Applied Physics Letters 88 (2006) 91915.

[116] R. Schaeublin, N. Baluc, Nuclear Fusion 47 (2007) 1690–1695.
[117] S.M. Hafez Haghighat, J. Fikar, R. Schaeublin, Journal of Nuclear Materials (2008), in press.
[118] V. Vitek, Philosophical Magazine 84 (2004) 415–428.
[119] R. Schaublin, Y.L. Chiu, Journal of Nuclear Materials 362 (2007) 152–160.
[120] Y.N. Osetsky, D.J. Bacon, Journal of Nuclear Materials 323 (2003) 268–280.
[121] Y.N. Osetsky, D.J. Bacon, Materials Science and Engineering A 400–401 (2005) 374–377.
[122] S.M. Hafez Haghighat, R. Schaeublin, Scientific Modeling and Simulation 14 (2007) 191–201.
[123] S.M. Hafez Haghighat, R. Schaeublin, Molecular dynamics modeling of cavity strengthening in irradiated iron, in: Proceedings of Multiscale Materials Modeling, Freiburg, 2006.
[124] W.R. Wampler, T. Schober, B. Lengeler, Philosophical Magazine 34 (1976) 129–141.
[125] K. Shiraishi, A. Hishinuma, Y. Katano, Radiation Effects and Defects in Solids 21 (1974) 161–164.
[126] C.C. Fu, F. Willaime, Physical Review B 72 (2005) 064117.
[127] W.D. Wilson, C.L. Bisson, M.I. Baskes, Physical Review B 24 (1981) 5616–5624.